David Reinisch, Bernhard Schmid, Nemanja Martić, Ralf Krause, Harald Landes, Marc Hanebuth, Karl J.J. Mayrhofer and Günter Schmid*

Various CO_2-to-CO Electrolyzer Cell and Operation Mode Designs to avoid CO_2-Crossover from Cathode to Anode

https://doi.org/10.1515/zpch-2019-1480
Received May 17, 2019; accepted October 24, 2019

Abstract: The electrochemical CO_2 reduction reaction (CO_2RR) towards CO allows to turn CO_2 and renewable energy into feedstock for the chemical industry. Previously shown electrolyzers are capable of continuous operation for more than 1000 h at high faradaic efficiencies and industrially relevant current densities. However, the crossover of educt CO_2 into the anode gas has not been investigated in current cell designs: Carbonates (HCO_3^- and CO_3^{2-}) are formed at the cathode during CO_2RR and are subsequently neutralized at the anode. Thus, CO_2 mixes into the anodically evolved O_2, which is undesired from commercial perspectives. In this work this chemical transport was suppressed by using a carbonate-free electrolyte. However, a second transport mechanism via physically dissolved gases became apparent. A transport model based on chemical and physical absorption of CO_2 and O_2 will be proposed and two solutions were experimentally investigated: the use of an anode GDL (A-GDL) and degassing the anolyte

***Corresponding author: Günter Schmid,** Siemens AG, Gas and Power, Power2X and Storage, Günter-Scharowsky-Str 1, 91058 Erlangen, Germany, e-mail: guenter.schmid@siemens.com
David Reinisch and Nemanja Martić: Siemens AG, Gas and Power, Power2X and Storage, Günter-Scharowsky-Str 1, 91058 Erlangen, Germany; and Department of Chemical and Biological Engineering, Friedrich-Alexander-Universität Erlangen-Nürnberg, Egerlandstr. 3, 91058 Erlangen, Germany
Bernhard Schmid: Forschungszentrum Jülich, Institute of Energy and Climate Research, Fundamental Electrochemistry (IEK-9), Ostring O10, 52425 Jülich, Germany
Ralf Krause, Harald Landes and Marc Hanebuth: Siemens AG, Gas and Power, Power2X and Storage, Günter-Scharowsky-Str 1, 91058 Erlangen, Germany
Karl J.J. Mayrhofer: Department of Chemical and Biological Engineering, Friedrich-Alexander-Universität Erlangen-Nürnberg, Egerlandstr. 3, 91058 Erlangen, Germany; and Helmholtz-Institute Erlangen-Nürnberg for Renewable Energy (IEK-11), Forschungszentrum Jülich, 91058 Erlangen, Germany

with a membrane contactor (MC). Both solutions further reduce the CO_2 crossover to the anode below 0.1 CO_2 for each cathodically formed CO while still operating at industrially relevant current densities of 200 mA/cm^2.

Keywords: CO_2 crossover; CO_2 electrolysis; CO_2 electrolyzer design; CO_2RR; electrochemical CO generation; electrochemistry; high current density.

1 Introduction

Photocatalysis offers a promising path to harvest solar energy and store it chemically for later utilization. The photocatalytic reduction of CO_2 furthermore helps reducing global CO_2 emissions and save fossil resources [1, 2]. CO_2 reduction products can be used as feedstock in the chemical industry or to generate synthetic fuels – and thus be easily integrated into existing infrastructure.

However, the direct photocatalytic reduction of CO_2 is at the current point in time not industrially applicable due to its low technology readiness level. An intermediate pathway is the generation of electricity from solar power and a subsequent electrochemical CO_2 reduction reaction (CO_2RR). The CO_2 can either be captured as a waste product from point sources, such as cement plants, refineries and ammonia production [3–5], or by direct air capture [6]. The variety of possible products ranges from CO, formate to C2 and C3 hydrocarbons [7]. CO_2RR is complex and a variety of factors influence its selectivity and efficiency. The choice of electrolyte and the local pH at the cathode surface play important roles [8–13]. A high pH value at the cathode helps to suppress the competing hydrogen evolution reaction (HER) due to sluggish kinetics.

For an industrial application, current densities above 200 mA/cm^2, lifetimes of several 10,000 h and an efficient utilization of energy and educts are essential [14]. The high current density puts additional constraints on the system as the properties at the electrode interfaces change locally. Hence, ionic liquids, that show great results at low current densities [15], decompose at the cathode due to the locally high alkalinity [16].

Among the different CO_2RR processes, the production of CO is especially close to meeting the industrial requirements and a promising candidate for implementation in the near future: Various stable catalysts have been identified, CO can be used in a variety of downstream processes and different studies have shown the economic and technological potential of electrochemical CO production [14, 17]. Various systems perform at high current densities using salt based liquid electrolytes or polymeric electrolytes in form of membranes [18, 19]. Furthermore, systems have been shown that can operate under these conditions for

more than 1000 h, while maintaining their selectivities [20–22]. However, until now the evaluation of electrolyzer designs has been mainly focused on selectivity, current density and the cathode potential [23]. But as these milestones have been achieved the focus needs to be widened. One of the so far overlooked challenges is the efficient utilization of the educt substrate CO_2.

2 Carbonate transport within the cell

The transport of CO_2 across the cell plays a critical role for industrialization. The neutralization of cathodically formed OH^- has been known for decades [24] and the neutralization of carbonates at the anode has been used to determine the main charge carrier through an anion exchange membrane [21]. Nonetheless, only recently this transport has been addressed as an issue for application in electrochemical CO_2RR in aqueous environments [25].

A schematic drawing of the process is given in Figure 1. In the initial reaction step at the cathode CO_2 is reduced to form CO and OH^- (Step 1):

$$CO_2 + H_2O + 2e^- \rightarrow CO + 2OH^- \tag{1}$$

OH^- might also be produced in the competing hydrogen evolution reaction:

$$2H_2O + 2e^- \rightarrow 2H_2 + 2OH^- \tag{2}$$

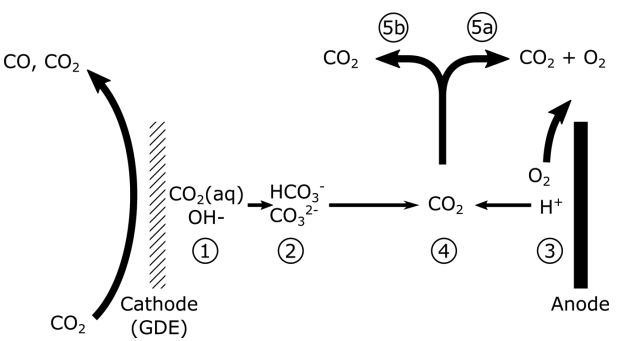

Fig. 1: Schematic diagram for the CO_2 crossover via cathodically formed carbonates. In the cathode reaction OH^- is produced (1) according to equations (1) and (2) which immediately reacts with physically dissolved CO_2 to form carbonates (2) [equations (3) and (4)]. Meanwhile H^+ is produced in the OER at the anode (3) (equation 5). When these two species meet, they neutralize and release CO_2 once again (4) [equations (6) and (7)]. If this neutralization occurs in the vicinity of the anode, the released CO_2 can mix with the anodically evolved O_2 (5a).

As CO_2 is present in the reaction zone, these OH^- can react quickly to form carbonates (Step 2) [26]:

$$OH^- + CO_2 \rightarrow HCO_3^- \tag{3}$$

$$2OH^- + CO_2 \rightarrow CO_3^{2-} + H_2O \tag{4}$$

The ratio of HCO_3^- and CO_3^{2-} depends on a variety of factors, such as the availability of CO_2 in the vicinity of the cathode, the rate of OH^- formation, and the mass transport in the electrolyte. The following discussion of the transport mechanism is similar for either of the species (HCO_3^- and CO_3^{2-}) and therefore they will be referred to as carbonates.

If the electrolyzer operates stable in a steady state these carbonates formed at the cathode cannot continuously accumulate but need to be neutralized. In all known high-current density electrolyzer designs H^+ is formed in the oxygen evolution reaction (OER) (Step 3) at the anode and neutralizes the carbonates (Step 4).

$$\text{OER: } H_2O \rightarrow \frac{1}{2}O_2 + 2H^+ + 2e^- \tag{5}$$

$$\text{Neutralization: } HCO_3^- + H^+ \rightarrow CO_2 + H_2O \tag{6}$$

$$\text{or } CO_3^{2-} + 2H^+ \rightarrow HCO_3^- + H^+ \rightarrow CO_2 + H_2O \tag{7}$$

The chemical absorption [equations (3) and (4)] and subsequent release [equations (6) and (7)] of CO_2 provides a transport route of CO_2 in the cell, that is driven by the electrochemical reactions. Even in an ideal cell with 100% Faraday efficiency for CO (FE_{CO}), one (via CO_3^{2-}) to maximum two (via HCO_3^-) CO_2 can be transported through the cell for each cathodically formed CO. For lower FE_{CO} this ratio can be even higher.

Current electrocatalysts for CO_2RR do not perform under acidic conditions. Therefore, in most cell designs the neutralization occurs near to the anode, so that the CO_2 from the neutralization reaction mixes with the O_2 from the OER (Step 5a). In this configuration the anode gas may contain between 66% (transport via CO_3^{2-}) and 80% (transport via HCO_3^-) CO_2. Such a CO_2-O_2-mixture is especially difficult to separate and thus recovering the CO_2 from the anode gas would not be practical. Hence, all CO_2 going to the anode should be considered as loss. However, if this mixing of O_2 and CO_2 can be avoided (Step 5b), the shuttled CO_2 can be reused. Therefore, controlling this CO_2 crossover is critical to ensure an efficient utilization of the CO_2 supplied to the electrolyzer.

3 Experimental section

The basic electrolyzer design is based on the work of Haas et al. [20] with the hereafter discussed modifications (Figure 2a). The CO_2RR was performed in a flow cell (ElectroCell) with an active electrochemical area of 10 cm^2. The cell consisted of three compartments (5 mL each): A cathode gas compartment, a catholyte compartment and an anolyte compartment. In experiments with an anode gas diffusion layer (A-GDL) an additional anode gas compartment was added to the cell (Figure 7a). The two electrolyte compartments were separated by a ZrO_2 based diaphragm, preventing convective mixing of electrolytes and gases between the two compartments. The cathode was a gas diffusion electrode made from Ag-nanoparticles and a hydrophobic binder polymer. For all CO_2 crossover experiments the selectivity for CO was above 90% at 200 mA/cm^2.

The anode was either an IrO_2-coated Ti sheet metal (ElectroCell) or an anode GDL (A-GDL). The A-GDL was prepared by dropcasting an ink prepared from 1-Propanol, 2 mg/cm^2 IrO_2 (Premion, Alfa Aesar) and 15 wt% Nafion as binder on a commercial, carbon-based gas diffusion layer (Freudenberg H23C2).

0.5 M K_2SO_4 (ACS, Alfa Aesar) or 1 M $KHCO_3$ (ACS, Alfa Aesar) were used as electrolyte. The solutions were prepared by dissolving the salt in ultrapure water (Milli-Q, Merck). For each electrolyte compartment, the electrolyte was drawn from a single electrolyte reservoir and pumped through the cell at a flow rate of

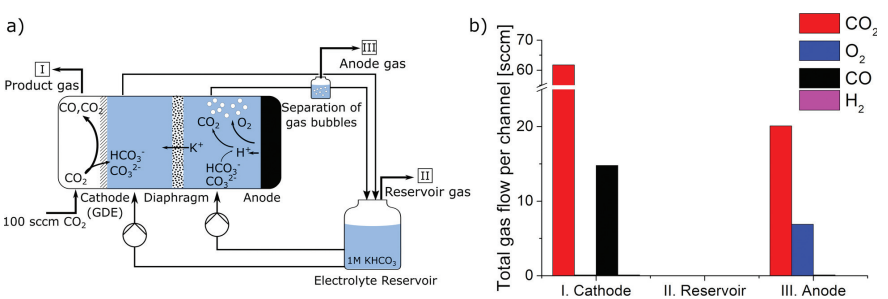

Fig. 2: (a) Electrolyzer with a mixed electrolyte designed after Haas et al. [20]. The catholyte and anolyte are drawn from a single electrolyte reservoir. A ZrO_2-based diaphragm separates the anolyte and catholyte compartment. After passing through the cell the anolyte and catholyte are remixed in the electrolyte reservoir, thus equalizing any concentration differences induced by the electrochemical reaction and the ionic current. Due to the presence of HCO_3^- in the anolyte, the CO_2 crossover to the anode gas is inherent to the system. Measurement of the gas composition per channel (b) therefore identifies CO_2 as the main component of the anode gas. As the neutralization occurs in the anolyte compartment there are no gases released from the reservoir.

100 mL/min. The size of the reservoir was 1 L to ensure sufficient retention time for reaching equilibrium. After passing through the cell any gas bubbles were separated from the anolyte and the two electrolyte streams were pumped back into the electrolyte reservoir (cp. experiments shown in Figures 2a, 3a, 6a). In the A-GDL experiment (Figure 7a) there were no gas bubbles visible in the anolyte channel and therefore gas bubble separation was not necessary.

During electrolysis 100 sccm (standard cubic centimeters per minute) CO_2 (4.5 N, Air Liquide) were supplied to the cathode gas compartment. With a PGSTAT302N potentiostat (Metrohm) in galvanostatic mode 2 A (200 mA/cm^2) were applied to the cell. At this current 15.2 sccm CO can be produced at the cathode.

In each experiment three gas flows were observed and measured: The "cathode gas" from the cathode gas compartment, the "reservoir gas" from the electrolyte reservoir and the "anode gas", from either the anode gas bubble separation or the anode gas compartment. The composition of the gas streams was measured with a Trace 1310 gas chromatograph (Thermo Scientific) equipped with two thermal conductivity detectors (TCD). For separation of CO_2, O_2 and CO a micropacked GC column (shin carbon) was used with a He carrier. The H_2 was separated with a packed mol-sieve column with Ar as carrier. The flow rates of the gas streams were quantified with either a drum style gas meter or a MilliGascounter (both Ritter). The three channels were connected to one gas chromatograph via a multiport valve. The total measurement cycle including analysis, purge and cooling took about 20 min. Thus, a full data point could be acquired in about 1 h.

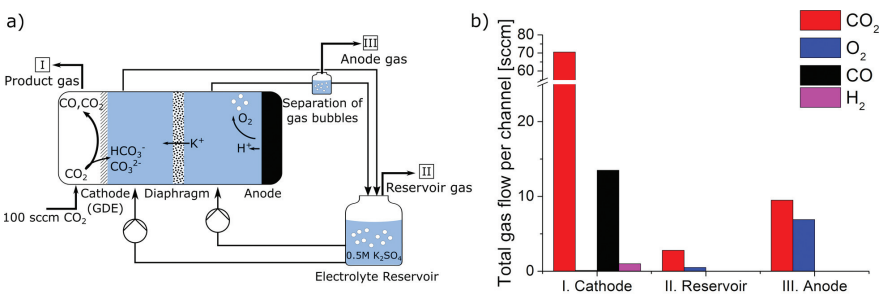

Fig. 3: (a) Electrolyzer with a K_2SO_4 electrolyte. The ionic current between catholyte and anolyte is predominately carried by K^+. Therefore, the catholyte accumulates carbonates, and the anolyte accumulates H^+. These neutralize when the two electrolyte streams are mixed in the electrolyte reservoir. Measurement of the gas flow per channel (b) shows that the CO_2 transport to the anode is reduced compared to the bicarbonate system (cp. gas composition in Figure 2b). However, CO_2 remains the main component of the anode gas. Furthermore, the presence of O_2 in the reservoir gas indicates, that the simple model of chemically bound CO_2 is not sufficient to explain these results.

The experiment was run for at least 1 h to ensure the system reached a steady-state, before the gas-streams were quantified and analyzed. During the experiment both the volumetric gas flows as well as the gas compositions for each channel remained stable. Three data points were averaged to one measurement requiring around 3 h.

4 Results and discussion

4.1 Investigation of crossover via carbonate neutralization

As a reference experiment the electrolyzer was operated with a bicarbonate electrolyte (1 M $KHCO_3$, experiment sketched in Figure 2a). In this system the anolyte and catholyte compartment are separated by a diaphragm which is permeable for cations and anions. However, it was experimentally proven, that the current is transported mainly by potassium ions and not by protons due to the huge concentration difference by seven orders of magnitude ($K^+ \sim 10^0$ mol/L and 10^{-7} mol/L, pH $\sim$ 7; experiment not included in this article). The protons formed at the anode by OER [equation (5)] react with HCO_3^- or CO_3^{2-} to gaseous CO_2 and H_2O [equations (6) and (7)]. The migrated K^+ are the counterions for the carbonates formed at the cathode by equations (1)–(4). It can be calculated, that the ion concentrations differ around $\sim$1% between the anolyte and catholyte after passing through the cell. The difference is equilibrated by re-mixing anolyte and catholyte after the cell in a single, large electrolyte reservoir. Such a system has the advantage that neither expensive ion-selective membranes nor a concentration management of the electrolytes is required. This electrolyzer design has already been proven to operate stable for more than 1000 h [20]. Carbonates are pumped into the anolyte compartment where they directly neutralize with H^+ from the OER. Therefore, a mixing of O_2 and CO_2 is inherent to this configuration. In contrast to ref. 20 all individual gas streams are analyzed. Figure 2b shows the gas distribution measured in the reference experiment. There was no gas evolution from the electrolyte reservoir, proving that the neutralization entirely occurred in the anolyte chamber. The measured composition of the anode gas was roughly 3:1 CO_2:O_2 with a total gas flow of 27 sccm. Therefore around 0.66 CO_2 for each e^- transferred in the electrochemical reaction reach the anode gas. This corresponds to a carbonate ratio of 2 CO_3^{2-}: 1 HCO_3^- from the cathode reaction. With a FE_{CO} above 90%, this equals to a transport and potential loss of up to $2 \cdot 0.66/0.9 \sim 1.5$ CO_2 for each cathodically produced CO.

Operating the electrolyzer with a carbonate-free electrolyte should avoid the neutralization of carbonates in the anolyte compartment and minimize the CO_2

crossover. However, the cathodic CO_2RR puts additional constraints on the electrolyte choice: in acidic media the HER becomes dominant, and in alkaline media the educt CO_2 reacts to carbonates both with OH^- from the reaction and additionally from the electrolyte [18, 26]. Thus, a neutral electrolyte [0.5 M K_2SO_4, pH = 6.3 after preparation, pH = 3–4 during operation, equation (5), absorption of CO_2] was chosen ("K_2SO_4" experiment).

Figure 3a sketches the experiment and shows the expected transport mechanism: At 2 A, $2.1 \cdot 10^{-5}$ mol/s of H^+ and HCO_3^- are formed in the electrolyte. With a flowrate of 100 mL/min the concentration of each species increases by 0.012 M during a single pass through the electrolyte compartment. This is negligible with respect to the ion concentrations of the 0.5 M K_2SO_4 but is reflected in a slight pH decrease of the anolyte. The ionic current between the two electrolyte compartments is mainly accomplished by the migration of K^+, similar to the $KHCO_3$ experiment. The H^+ and the carbonates are therefore transported by pumping to the electrolyte reservoir. The electrolyte retention time in the reservoir is 5 min and therefore long enough to allow the system to approach the thermodynamic equilibrium ($k = 2.67 \cdot 10^4 \frac{kg}{mol \cdot s}$ for equation (6) [27]). At the experimentally observed pH-value of 3–4 in the electrolyte reservoir, the equilibrium concentration of HCO_3^- is small. Hence, there is no significant carbonate concentration in the anolyte compartment, that can neutralize the anodically formed H^+. Therefore, the gas bubbles evolving in the anolyte compartment should consist mainly of O_2 instead of CO_2. In the electrolyte reservoir the anodically formed H^+ neutralizes with the cathodically formed carbonates and CO_2 is released there. Separating the O_2-rich gas from the anolyte before it reaches the reservoir, should therefore prevent a mixing of CO_2 and O_2. Such a system needs three gas outlets: the cathode gas, the anode gas and a reservoir gas from the electrolyte reservoir. Figure 3b shows the composition of the gas streams measured in this experiment. Even though the partial CO_2 flow in the anode gas is reduced from 20.1 sccm to 9.5 sccm, CO_2 still remains the major component of the anode gas (6.9 sccm O_2). This falls short of the expectations and moreover, the total gas flow from the reservoir is comparatively small (3.3 sccm), consists mainly of CO_2 (2.8 sccm), but contains non-negligible amounts of O_2 (0.5 sccm), too.

4.2 Crossover via physically dissolved gases

The simple straight forward model regarding ion migration and immediate chemical reactions needs to be refined. It is important to note that the system so far only accounts for the evolution of CO_2 and O_2 and neglects the distinction between gas bubbles and physically dissolved gases. If this is considered a new transport model (sketched in Figure 4) becomes apparent:

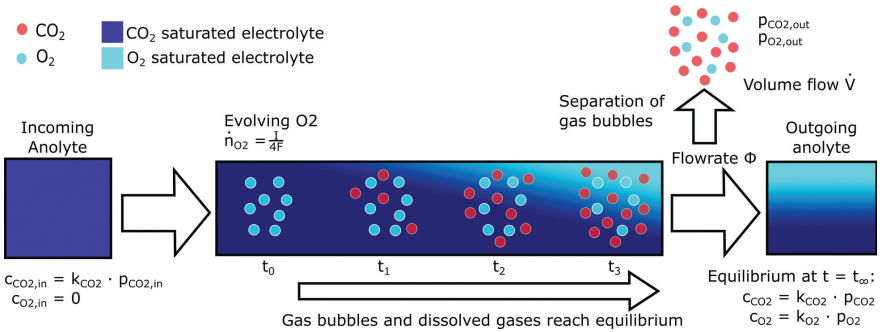

Fig. 4: Schematic drawing of the CO_2 transport via dissolved gases. Initially CO_2 is physically dissolved in the anolyte, while O_2 bubbles are evolved at the anode and carried along with the anolyte. As long as the bubbles are in contact with the anolyte, O_2 can physically dissolve and thereby release CO_2. As CO_2 is more soluble in aqueous media, more CO_2 is released than O_2 dissolves into the anolyte.

CO_2 can physically dissolve into the electrolyte at the cathode and as well originate from the neutralization reaction in the electrolyte reservoir. At standard conditions the maximum solubility of CO_2 in water is 0.034 M [28]. It is assumed, that the electrolyte in the reservoir is saturated to a degree s with CO_2:

$$c_{CO_2,res} = s \cdot k_{CO_2} \cdot p_{cell} \tag{8}$$

where $c_{CO_2,res}$ is the concentration of physically dissolved CO_2 in the electrolyte reservoir, k_{CO_2} is the Henry constant for CO_2 and p_{cell} is the total pressure in the electrolyzer. Therefore, as the anolyte is pumped from the electrolyte reservoir into the anolyte compartment, physically dissolved CO_2 can be carried along.

O_2 gas bubbles evolve at the anode and can physically dissolve as long as they are in contact with the anolyte. Here, they may replace previously physically dissolved CO_2, leading to a kind of equilibrium visualized by equation (9).

$$O_2(g) + xCO_2(aq) \rightleftarrows O_2(aq) + xCO_2(g) \tag{9}$$

At room temperature the solubility of CO_2 in water is 26-times higher than the solubility of O_2 [28, 29]. Therefore O_2 can release significantly larger quantities of CO_2 when it dissolves into the electrolyte ($x \gg 1$). When the gas bubbles are separated, the physically dissolved gases remain in the anolyte and are transported to the electrolyte reservoir. Here the catholyte and anolyte are mixed, and CO_2 is chemically evolved from the neutralization of carbonates and H^+. This CO_2 changes the equilibrium between the physically dissolved gases and therefore O_2

can be released from the electrolyte reservoir, leading to the more complex model shown in equations (10) and (11).

Neutralization:

$$\begin{aligned} &HCO_3^- + H^+ + x_1O_2(aq) + (y_1 - 1)CO_2(aq) \\ &\rightleftarrows \underbrace{y_1CO_2(aq) + x_1O_2(aq)}_{\text{exceed physical solubility}} + H_2O \end{aligned} \tag{10}$$

Release of gases:

$$\begin{aligned} &y_1CO_2(aq) + x_1O_2(aq) \\ &\rightarrow y_2CO_2(aq) + x_2O_2(aq) \\ &\quad + (y_1 - y_2)CO_2(g) + (x_1 - x_2)O_2(g) \end{aligned} \tag{11}$$

4.3 Modelling the crossover via physically dissolved gases

This transport mechanism can be approximated with a simple model based on the following assumptions:

- The anolyte is pumped through the anolyte compartment with a flowrate ϕ.
- The incoming anolyte is saturated with CO_2 to a degree s, with $p_{CO_2,in} = p_{CO_2,res} = s \cdot p_{cell}$, where $p_{CO_2,in}$ is the partial pressure of CO_2 at the anolyte inlet and p_{cell} is the total pressure in the cell and the concentration of dissolved CO_2 at the anolyte inlet is $c_{CO_2,in} = k_{CO_2} \cdot p_{CO_2,in}$.
- No other gases are physically or chemically dissolved in the incoming anolyte. This is an adequate approximation, since in the electrolyte (pH $\leq$ 4), the concentration of HCO_3^- from the CO_2/HCO_3^- equilibrium can be neglected.
- In the anolyte compartment O_2 is released at a rate of $\frac{I}{4F}$ where I is the total current applied and F is the Faraday constant. No other gases are evolved in the anolyte compartment.
- When the gas bubbles are separated from the outgoing electrolyte, they are in equilibrium with the physically dissolved gases:

$$c_{CO_2} = k_{CO_2} \cdot p_{CO_2} \tag{12}$$

$$c_{O_2} = k_{O_2} \cdot p_{O_2} \tag{13}$$

where c_{CO_2} and c_{O_2} are the concentrations of physically dissolved CO_2 and O_2, k_{CO_2} and k_{O_2} are the respective Henry constants, and p_{CO_2}, p_{O_2} are the respective partial pressures in the gas phase. This is an idealized approximation that would require infinite contact time. In the experiment the partial pressure

of CO_2 will remain lower ($p_{CO_2,real} \leq p_{CO_2}$) and the concentration of physically dissolved O_2 will also be slightly lower ($c_{O_2,real} \leq c_{O_2}$) than the values calculated from this model. It will be shown, that this assumption is sufficient for the model.

- The gas separated at the anolyte outlet has a volumetric flowrate $\dot{V}$ and only contains CO_2 and O_2:

$$p_{CO_2} + p_{O_2} = p_{cell} \tag{14}$$

where p_{cell} is the total pressure in the cell.

- No oversaturation occurs: $p_{O_2}, p_{CO_2}, p_{CO_2,in} \leq p_{cell}$

Based on these assumptions an equation system can be built upon the principle of conservation of mass:

$$\dot{n}_{O_2} = \frac{p_{O_2}}{p_{cell}} \frac{\dot{V}}{V_m} + p_{O_2} k_{O_2} \phi = \frac{I}{4F} \tag{15}$$

$$\dot{n}_{CO_2} = \frac{p_{CO_2}}{p_{cell}} \frac{\dot{V}}{V_m} + p_{CO_2} k_{CO_2} \phi = p_{CO_2,in} k_{CO_2} \phi \tag{16}$$

where V_m is the molar standard gas volume. This equation system can be solved analytically:

$$p_{CO_2} = \frac{\alpha\, p_{cell} + \dot{n}_{CO_2} + \dot{n}_{O_2} - \sqrt{(\alpha\, p_{cell} + \dot{n}_{CO_2} + \dot{n}_{O_2})^2 - 4\,\alpha\, p_{cell} \dot{n}_{O_2}}}{2\alpha} \tag{17}$$

$$p_{O_2} = \frac{\alpha\, p_{cell} - \dot{n}_{CO_2} - \dot{n}_{O_2} + \sqrt{(\alpha\, p_{cell} - \dot{n}_{CO_2} - \dot{n}_{O_2})^2 + 4\,\alpha\, p_{cell} \dot{n}_{CO_2}}}{2\alpha} \tag{18}$$

$$\dot{V} = \left(\frac{\dot{n}_{O_2}}{p_{O_2}} - k_{O_2} \phi \right) \cdot p_{cell} \cdot V_m = \left(\frac{\dot{n}_{CO_2}}{p_{CO_2}} - k_{CO_2} \phi \right) \cdot p_{cell} \cdot V_m \tag{19}$$

where $\alpha = \Phi(k_{CO_2} - k_{O_2})$.

The model was applied to the values listed in Table 1 and the saturation s was varied between 0 and 1. Figure 5a shows the resulting anode gas composition as a

Tab. 1: Values used for modelling the transport via physically dissolved gases.

Φ	100 $\frac{mL}{min}$	k_{O_2}	1.3×10^{-3} $\frac{mol}{L \cdot bar}$
T	25 °C	p_{cell}	1013 mbar
I	2 A	$p_{CO_2,in}$	$s \cdot p_{cell}$
k_{CO_2}	0.034 $\frac{mol}{L \cdot bar}$	$p_{O_2,in}$	0 mbar

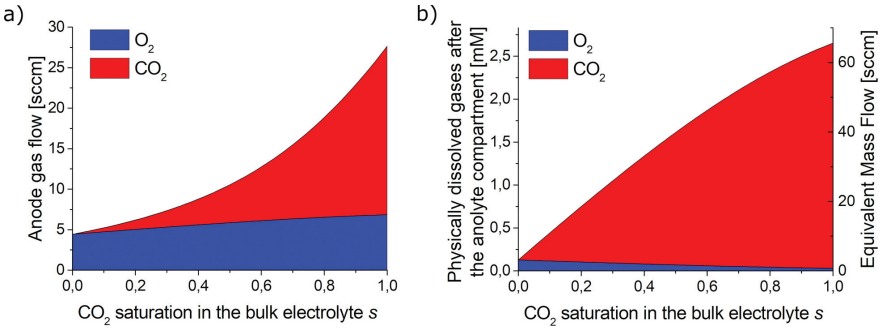

Fig. 5: (a) Calculated anode gas composition assuming the gas phase and the physically dissolved gases are in equilibrium. The calculations are based on equations (17)–(19) and the parameters listed in Table 1. The calculation shows that this model can explain anode gas compositions where CO_2 exceeds the O_2 content. Calculation of the physically dissolved gases in the anolyte after passing through the cell (b) shows that O_2 can dissolve into the anolyte. Therefore, physically dissolved O_2 can be transported from the anolyte compartment to the electrolyte reservoir, explaining the presence of O_2 in the reservoir gas. The measured gas compositions from the carbonate-free system (Figure 3b), would correspond to a CO_2 saturation $s \approx 0.8$.

function of s. As the incoming CO_2 saturation s increases, more CO_2 gets released in the anode gas. For saturation levels $s > 0.57$, CO_2 is the main constituent of the anode gas. Figure 5b shows the corresponding concentration of physically dissolved gases in the anolyte after separation of the gas bubbles. Here, some of the anodically evolved O_2 dissolves into the anolyte and is missing from the anode gas. This fits with the experimental observations and thus the proposed mechanism of chemically and physically dissolved gas can indeed fully explain the observed gas compositions in carbonate and non-carbonate-based electrolytes.

4.4 Reducing the crossover via physically dissolved gases

Two further paths can be derived from the model to reduce CO_2 transport through the cell even more. Reduction of the CO_2 saturation of the incoming anolyte will shift the equilibrium. Reduction of the contact time between the gas bubbles and the anolyte will prevent the system from reaching the equilibrium, calculated by the model.

4.4.1 Reduction of the CO_2 saturation of the incoming anolyte

As shown by the model calculations (Figure 5a) reducing the saturation s will also reduce the CO_2 flow in the anode gas. However, as a tradeoff for low s more O_2 can

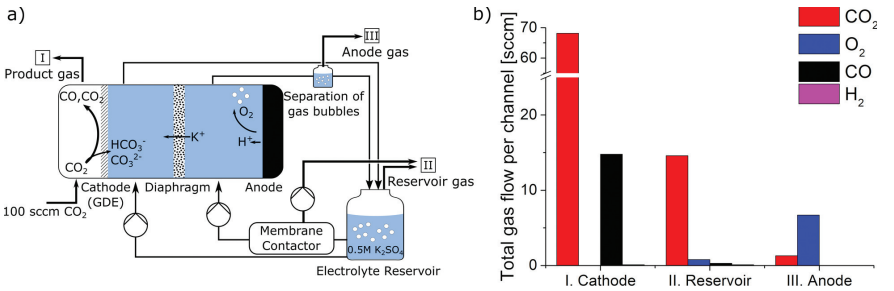

Fig. 6: (a) Electrolyzer with a membrane contactor (MC): prior to entering the cell the anolyte passes through a MC that is operated at 250 mbar and thereby physically dissolved gases are removed from the anolyte. These gases are then added to the reservoir gas (II). Otherwise this design is identical to the design shown in Figure 3a. Measurement of the gas flow per channel (b) shows that the CO_2 crossover to the anode is significantly reduced (1.3 sccm) compared the previous experiments (cp. gas composition in Figure 2b, 3b). However, the partial O_2 flow in the reservoir gas increased to 0.8 sccm.

dissolve into the anolyte and potentially be released in the reservoir. For experimental verification a membrane contactor (MC) (Liqui-Cel 1.7 × 5.5, 3 M, suited for flows up to 2500 mL/min [30]) was inserted between the reservoir and the anolyte compartment ("MC" experiment, design shown in Figure 6a). The membrane contactor was connected to a vacuum pump and operated at 250 mbar. It was expected that the CO_2 saturation s in the anolyte compartment can be reduced to 0.25 at 250 mbar. The gas separated by the membrane contactor was then combined with the reservoir gas for analysis.

The partial CO_2 flow in the anode gas was reduced from 9.5 sccm to 1.3 sccm (0.045 CO_2 per e^-), while the partial CO_2 flow in the reservoir gas increased from 2.1 sccm to 14.6 sccm, compared to the experiment with a K_2SO_4 electrolyte. As predicted by the model the partial O_2 flow in the reservoir gas increases from 0.6 sccm to 0.8 sccm.

4.4.2 Reduction of the contact time between the gas bubbles and the anolyte

The second possibility to reduce the crossover via physically dissolved gases is to separate the gas bubbles from the electrolyte before an equilibrium can be reached. Thereby, the dissolution of O_2 into the anolyte is limited and the system is kept at its original and ideal state (physically dissolved CO_2 in the anolyte and O_2 in the gas phase, cp. $t = t_0$ in Figure 4).

Experimentally the solid anode was replaced by a gas diffusion anode ("A-GDL" experiment, design shown in Figure 7a). The hydrophobic backbone of the A-GDL absorbs the gas bubbles formed on the anode surface and transfers them

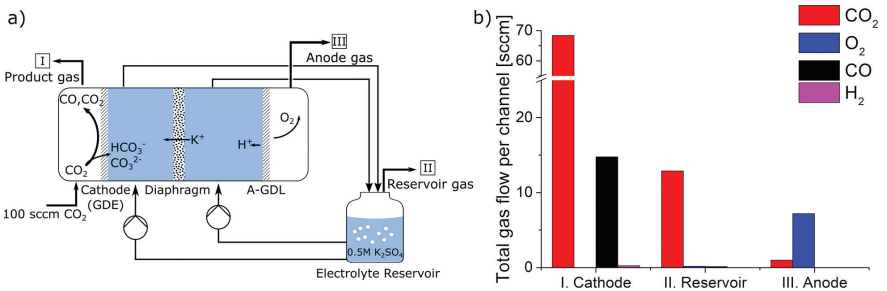

Fig. 7: (a) Electrolyzer with an anode GDL (A-GDL). The solid anode is replaced by an A-GDL and an anode gas compartment is added to the cell. In such a configuration the anodically evolved O_2 is transported through the A-GDL into the anode gas compartment and the anode gas (III) is collected there. There were no gas bubbles observed in the anolyte coming from the cell and thus the separation of gas bubbles is not necessary. Measurement of the gas flow per channel (b) shows that the CO_2 crossover to the anode is reduced to 1.0 sccm and the partial O_2 flow in the reservoir gas is reduced to 0.2 sccm.

to the anode gas compartment. No gas bubbles were observed in the electrolyte. The interaction between the gas phase and the electrolyte occurs only on the surface of the A-GDL. The Nafion in the catalyst layer of the A-GDL is used as a binder and does not act as an ion conducting membrane. An experiment with a $KHCO_3$ electrolyte and an A-GDL did not prevent mixing of CO_2 and O_2 (experiment not shown here).

The distribution of gas flows and their composition for this experiment is shown in Figure 7b. The partial CO_2 flow in the anode gas drops from 9.5 sccm to 1.0 sccm (0.033 CO_2 per e^-) and the O_2 content in the electrolyte reservoir drops from 0.6 sccm to 0.2 sccm, which is in good agreement with the model.

The measured and calculated gas compositions are summarized in Figure 8. Figure 8a displays the anode gas compositions, whereas Figure 8b contains the reservoir gas compositions.

- The reference experiment with a mixed $KHCO_3$ electrolyte showed the highest CO_2 partial flow of 20.1 sccm in the anode gas. No reservoir gas could be observed.
- Changing to a K_2SO_4 electrolyte reduced the CO_2 crossover to the anode by over 50%. The high partial CO_2 flow (9.5 sccm) can be explained by taking physical solubility into account [equations (9)–(11)]. There is only little gas evolution (2.1 sccm CO_2, 0.6 sccm O_2) from the reservoir. The data for this experiment agrees well with the model assuming a CO_2 saturation $s = 0.8$.
- Degassing with a membrane contactor (MC) reduced the CO_2 crossover to the anode by 85% to a value of 1.3 sccm compared to the K_2SO_4 experiment. The O_2 crossover to the reservoir gas increased from 0.6 sccm to 0.8 sccm. These

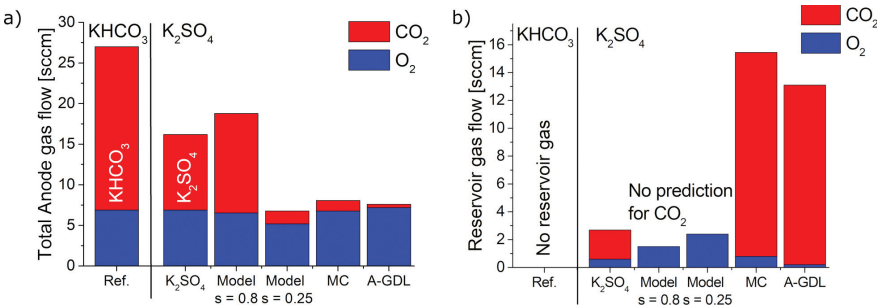

Fig. 8: Comparison of gas composition from experimental data and estimations from the model. (a) Composition of the anode gas. Compared to the $KHCO_3$ system, a K_2SO_4 electrolyte reduces the CO_2 flow in the anode gas by more than 50%. The remaining CO_2 in the anode gas fits to the values predicted by the model ($s = 0.8$). Degassing with a membrane contactor (MC) or an A-GDL reduced the CO_2 crossover even further. The data from the MC experiment agrees well with the calculations of the model ($s = 0.25$). (b) Composition of the reservoir gas. With a $KHCO_3$ electrolyte the neutralization occurs in the anolyte compartment and no reservoir gas was observed. The K_2SO_4 electrolyte shifted the neutralization reaction to the reservoir and gas evolution was observed from the reservoir. However, there is still a significant O_2 contribution to the anode gas (22%). The CO_2:O_2 ratio in the reservoir gas was increased, both in the MC and the A-GDL experiment. With a MC partial O_2 flow increased as predicted by the model (comparison of $s = 0.8$ and $s = 0.25$). In contrast, the A-GDL reduced the partial O_2 flow in the reservoir gas.

results agree with the predictions of the calculations (comparison of $s = 0.8$ and $s = 0.25$).

– The introduction of an A-GDL, reduced the CO_2 crossover to the anode gas by almost 90% compared to the K_2SO_4 experiment and over 95% compared to the reference experiment. The lowest CO_2 partial flow for all experiments was measured (1.0 sccm). The O_2 crossover to the reservoir gas was reduced to 0.2 sccm.

5 Conclusion

As CO_2RR research advances towards application, challenges beyond selectivity and electric efficiency need to be solved. The crossover of CO_2 from cathode to anode is one of the key issues for CO_2RR in aqueous media. Current CO_2RR electrocatalysts require alkaline conditions and therefore carbonates are formed as by-products at the cathode and commonly neutralized in the vicinity of the anode. The resulting release of CO_2 puts industrially relevant constraints onto the design of a CO_2 electrolyzer and its operating conditions. Using a sulfate-based, mixed electrolyte offers in principle a simple way to control the transport of carbonates

in aqueous electrolytes. However, the high physical solubility of CO_2 in aqueous media can introduce a new pathway for CO_2 transport across the cell. A simple model of the equilibrium between physically and chemically dissolved CO_2 and physically dissolved O_2 is sufficient to explain the gas distribution for the sulfate-based, mixed electrolyte. Degassing the electrolyte with a membrane contactor (MC) or introducing an anode GDL (A-GDL) reduced the CO_2 crossover even further. The MC decreased the CO_2 saturation and thus, caused the equilibrium between the dissolved gases to shift. The A-GDL helped to remove the evolving O_2 immediately from the anolyte compartment, and therefore prevented the system from reaching its equilibrium. With an A-GDL the CO_2 transport across the cell could be reduced by over 95% compared to the reference experiment with a $KHCO_3$ electrolyte, while maintaining Faraday efficiencies higher than 90% and operating stable at current densities of 200 mA/cm^2. In the future these results will be further improved by optimizing the operation conditions such as increasing temperature.

References

1. O. Ola, M. M. Maroto-Valer, J. Photochem. Photobiol. C **24** (2015) 16.
2. A. Dominguez-Ramos, A. Irabien, Sustainable Prod. Consumption **17** (2019) 229.
3. M. Finkenrath, IEA Energy Papers (2011).
4. R. T. J. Porter, M. Fairweather, C. Kolster, N. Mac Dowell, N. Shah, R. M. Woolley, Int. J. Greenhouse Gas Control **57** (2017) 185.
5. N. von der Assen, L. J. Müller, A. Steingrube, P. Voll, A. Bardow, Environ. Sci. Technol. **50** (2016) 1093.
6. K. Z. House, A. C. Baclig, M. Ranjan, E. A. van Nierop, J. Wilcox, H. J. Herzog, Proc. Natl. Acad. Sci. U.S.A. **108** (2011) 20428.
7. Y. Hori, H. Wakebe, T. Tsukamoto, O. Koga, Electrochim. Acta **39** (1994) 1833.
8. O. Ayemoba, A. Cuesta, ACS Appl. Mater. Interfaces **9** (2017) 27377.
9. A. Wuttig, Y. Yoon, J. Ryu, Y. Surendranath, J. Am. Chem. Soc. **139** (2017) 17109.
10. S. Verma, X. Lu, S. Ma, R. I. Masel, P. J. A. Kenis, Phys. Chem. Chem. Phys. **18** (2016) 7075.
11. J. E. Pander, D. Ren, Y. Huang, N. W. X. Loo, S. H. L. Hong, B. S. Yeo, ChemElectroChem **5** (2018) 219.
12. Y. Pang, T. Burdyny, C.-T. Dinh, M. G. Kibria, J. Z. Fan, M. Liu, E. H. Sargent, D. Sinton, Green Chem. **19** (2017) 4023.
13. J. Resasco, L. D. Chen, E. Clark, C. Tsai, C. Hahn, T. F. Jaramillo, K. Chan, A. T. Bell, J. Am. Chem. Soc. **139** (2017) 11277.
14. M. Jouny, W. Luc, F. Jiao, Ind. Eng. Chem. Res. **57** (2018) 2165.
15. B. A. Rosen, A. Salehi-Khojin, M. R. Thorson, W. Zhu, D. T. Whipple, P. J. A. Kenis, R. I. Masel, Science **334** (2011) 643.
16. S. S. Neubauer, B. Schmid, C. Reller, D. M. Guldi, G. Schmid, ChemElectroChem **4** (2017) 160.
17. J. M. Spurgeon, B. Kumar, Energy Environ. Sci. **11** (2018) 1536.

18. C.-T. Dinh, F. P. García de Arquer, D. Sinton, E. H. Sargent, ACS Energy Lett. **3** (2018) 2835.
19. D. M. Weekes, D. A. Salvatore, A. Reyes, A. Huang, C. P. Berlinguette, Acc. Chem. Res. **51** (2018) 910.
20. T. Haas, R. Krause, R. Weber, M. Demler, G. Schmid, Nat. Catal. **1** (2018) 32.
21. J. J. Kaczur, H. Yang, Z. Liu, S. D. Sajjad, R. I. Masel, Front. Chem. **6** (2018) 263.
22. R. B. Kutz, Q. Chen, H. Yang, S. D. Sajjad, Z. Liu, R. I. Masel, Energy Technol. **5** (2017) 929.
23. O. S. Bushuyev, P. de Luna, C.-T. Dinh, L. Tao, G. Saur, J. van de Lagemaat, S. O. Kelley, E. H. Sargent, Joule **2** (2018) 825.
24. Y. Hori, A. Murata, T. Ryutaro, J. Chem. Soc. Faraday Trans. **1** (1989) 2309.
25. A. Pătru, T. Binninger, B. Pribyl, T. J. Schmidt, J. Electrochem. Soc. **166** (2019) F34.
26. B. Schmid, C. Reller, S. Neubauer, M. Fleischer, R. Dorta, G. Schmid, Catalysts **7** (2017) 161.
27. K. G. Schulz, U. Riebesell, B. Rost, S. Thoms, R. E. Zeebem, Mar. Chem. **100** (2006) 53.
28. J. J. Carroll, J. D. Slupsky, A. E. Mather, J. Phys. Chem. Ref. Data **20** (1991) 1201.
29. H. L. Clever, R. Battino, H. Miyamoto, Y. Yampolski, C. L. Young, J. Phys. Chem. Ref. Data **43** (2014) 33102.
30. 3M™ Liqui-Cel™ MM-1.7x5.5 Series Membrane Contactor Datasheet, available at "https://multimedia.3m.com/mws/media/1412492O/3m-liqui-cel-mm-1-7x5-5-series-membrane-contactorlc-1007-pdf.pdf".